MPC-based path tracking with PID speed control for autonomous vehicles

MPC-based path tracking with PID speed control for autonomous vehicles

Shuping Chen[1], Huiyan Chen

School of Mechanical Engineering, Beijing Institute of Technology, Beijing 100081, China

[1] Email: 196747875@qq.com

Abstract. In this paper, a new coupled lateral and longitudinal controller based on model predictive control (MPC) framework was proposed for an autonomous vehicle to track the desired trajectory and speed. Considering the constraints of control input limit and state output admissible, we used a spatial-based 8 degrees of freedom (DOF) vehicle model as the prediction model and used a high-fidelity model, i.e., a 14-DOF vehicle model as the plant model in the formulation of MPC algorithm. For the lateral control, the MPC controller generates the optimal road-wheel steering angle; for the longitudinal control, the PID controller embedded in the optimization solution generates the total driving or braking wheel torque. All these control inputs were passed to the plant simultaneously. The developed vehicle models were simulated with step steering input and compared with the simulation result of CarSim vehicle model for validation. We implemented the proposed controller for path tracking and speed control with MATLAB considering an 8-shaped curved trajectory as the reference. The simulation results showed that the path tracking and speed tracking performance were good using the combined lateral and longitudinal control strategy.

1. Introduction

With the advancement in computer and sensor technology, autonomous vehicles which ensure reliable and safe navigation without driver control and continuous monitoring, have received worldwide attention and rapid development during last decades, not only in the research field, but also in the industrial, academic and military fields. Several competitions such as the DARPA (Defense Advanced Research Projects Agency) Challenges in the USA; the Korean Autonomous Vehicle Competitions (AVC) in Korea; the Intelligent Vehicle Future Challenge of China and many other contests have been held to advance the development of autonomous vehicles [1,2].

Driving control including lateral control and longitudinal control is one of the core issues in the research of autonomous vehicles. The lateral control aims to track the desired trajectory and heading angle, while the longitudinal control aims to track the desired speed. To this end, various controllers have been developed via classical control theory, modern control theory and robust control theory, etc. such as PID control [3,4], optimal control [5,6], robust backstepping and sliding mode control [7,8], etc. However, these control methods did not consider the actuator saturation and physical limit. Model predictive control, which combines prediction model, receding horizon optimization and feedback correction, has advantages to handle these issues due to its consideration of input constraints and state admissible [9]. Recent research shows that MPC algorithm is useful to control the dynamics of multiple vehicles considering safety constraints and the stability of these algorithms is also well studied [10]. An MPC-based path tracking controller considering the handling stability and

environmental constraints was proposed in [2] to address the complicated nonlinear constraints of sideslip and rollover in motion planning and path following for high-speed autonomous vehicles; A path following control scheme considering yaw and lateral stabilization for obstacle avoidance was proposed in [11] using combined steering and braking, in which a full tenth-order vehicle model and a simplified bicycle model were used respectively for nonlinear model predictive control (NMPC) formulation; An NMPC controller was introduced in [12] for path tracking with consideration of input limit and state output constraints by controlling the wheel steering, driving and braking and the NMPC algorithm was transformed to a linear model predictive control (LMPC) based on online linearization in order to reduce the computational burden. However, in the above studies, the lateral and longitudinal control were studied in a decoupled way. It is assumed that the longitudinal velocity was constant in the path tracking controller design. On the other hand, the coupling with the lateral dynamics was not taken into account when dealing with the longitudinal control [13]. The automotive vehicle can be treated as nonlinear system with varied parameters and strong couplings between the lateral and longitudinal dynamics. Actually, the vehicle speed is usually varied along the path according to the road information. For example, when the vehicle is entering a curve with small radius, it needs to reduce the speed to avoid large lateral acceleration to ensure safety; When the vehicle drives out of a curve and runs on a straight road, it needs to increase the speed to go through the road as fast as possible. Hence, a time varied speed should be considered in path tracking and a combination of the lateral and longitudinal control is quite necessary to improve the tracking performance due to the difficulty of handling the complicated traffic environment with separate controller [14].

We aim at designing a coupled lateral and longitudinal controller, it is therefore essential for us to identify the different coupling effects. The lateral and longitudinal dynamics coupling effects fall into three levels: kinetic coupling, tire force coupling and weight shift coupling. An example of kinetic coupling effect is that the lateral cornering force of front wheel has a component in the longitudinal direction; Tire force coupling effect can be described that given a coefficient of friction, the magnitude of the resultant of lateral and longitudinal forces on each tire is limited by a function of the direction of the resultant; Weight shift coupling effect can be shown that longitudinal acceleration affects the lateral dynamics by redistributing the tire normal forces, while lateral acceleration changes the weight distribution between the left and right tires [15,16]. In the literature, some approaches have been proposed to address the problem of controlling the lateral and longitudinal vehicle dynamics in a coupled way: for instance, a combined lateral and longitudinal controller based on sliding mode control theory was proposed in [17] to deal with these coupling effects; A flatness-based nonlinear controller was introduced in [18] for path tracking using combined lateral and longitudinal vehicle control; An integrated controller based on backstepping approach was presented in [19] for lane change and collision avoidance. In [20], a coupled longitudinal and lateral controller based on nonlinear backstepping theory and adaptive sliding mode control technique was proposed for automated driving control in emergency obstacle avoidance. In [21], an integrated control method including a spatial-based predictive control and geometric corridor planning was proposed for adaptive cruise control coupled with obstacle avoidance. Another integrated control scheme of adaptive cruise control with auto-steering was presented in [22] to design safe interaction between lateral and longitudinal controllers based on a proper logic-based control strategy. In [23], two coupled controllers were presented to tackle the challenge of lateral and longitudinal coupling effects: one was developed using Lyapunov control theory while the other one was based on Immersion and Invariance with sliding mode control. The model used in the controller design was four-wheel vehicle model using multi-body formalism based on Euler-Lagrange algorithm.

In this paper, in order to realize the coupled longitudinal and lateral control, we propose a novel MPC-based path tracking strategy with PID speed control for autonomous vehicles considering the constraints of input limit and output state admissible. The varied longitudinal velocity will be considered in the formulation of model predictive control algorithm. For the lateral control, we use MPC approach to generate the optimal road-wheel steering angle; for the longitudinal control, we use

PID controller embedded in the solution to generate the total acceleration or braking wheel torque. All the control inputs are passed to the plant simultaneously to track the reference path and desired speed. We use a double-track spatial-based 8-DOF vehicle model considering roll dynamics as the prediction model and a higher fidelity model, i.e., a 14-DOF vehicle model as the plant, since an accurate vehicle model is essential for the development of automotive control system. Moreover, to investigate the performance of the proposed controller in curved road situation, we consider an 8-shaped curved path as the reference.

The remainder of this paper is organized as follows: In Section 2, we described the tire model, an 8-DOF vehicle model, a 14-DOF vehicle model and a spatial-dependent vehicle model; In Section 3, we specified the MPC algorithm for path tracking and the PID controller for speed tracking; In Section 4, we first compared the simulation results of step steer response between the developed vehicle models and the CarSim vehicle model for validation; Then, we implemented the proposed controller for combined path tracking and speed control considering the references path to be an 8-shaped curve trajectory; In Section 5, we summarized the paper and outlined the future work.

2. Models for control synthesis

Since models are central to the formulation of model predictive control algorithm, we firstly present the development of vehicle dynamics models in this section including a linear tire model, an 8-DOF vehicle model, a 14-DOF vehicle model and a spatial-dependent vehicle model.

2.1. Tire model

Except for aerodynamics forces and gravity, all of the forces which affect vehicle behavior are provided by the tires. Because tire forces produce primary external influence and they have highly nonlinear performance, it is essential to use a realistic tire model, especially when investigating large control inputs that results in response near the limits of the linear character scale of the tire. The tire lateral and longitudinal forces are assumed to depend on normal force, slip angle, surface friction, and slip ratio. However, when the slip ratio and slip angle are limited within small values, the tire model can be simplified and generate linearized lateral force and longitudinal force [11,24].

Under this assumption, the tire lateral force can be given as $F_c = C_\alpha(\mu, F_z)\alpha$, where α is the tire slip angle, C_α is tire cornering stiffness related to tire normal force F_z and road-tire friction coefficient μ; The tire longitudinal force can be given as $F_l = C_x(\mu, F_z)s_{f,r}$, where $s_{f,r}$ is the slip ratio of front tire or rear tire, C_x is the tire longitudinal stiffness which also related to the tire normal force and road-tire friction coefficient.

2.2. 8-DOF vehicle model

When studying vehicle handling performance in the situations that do not involve large longitudinal accelerations, we usually used an 8-DOF vehicle model as a simplified lower order model to consider the vehicle roll dynamics. The 8-DOF model considers longitudinal, lateral, yaw and roll dynamics for the chassis and each wheel rotational dynamics without the pitch and heave motions [25]. The 8-DOF full vehicle model is shown in Figure 1.

The equation of chassis for the 8-DOF vehicle model according to Newton's laws are given as:

$$m_t(\dot{u} - \omega_z v) = \sum F_{xgij} + \left(m_{uf}a - m_{ur}b\right)\omega_z^2 - 2h_{rc}m\omega_z\omega_x \tag{1}$$

$$m_t(\dot{v} + \omega_z u) = \sum F_{ygij} + \left(m_{ur}b - m_{uf}a\right)\dot{\omega}_z + h_{rc}m\dot{\omega}_x \tag{2}$$

$$J_z\dot{\omega}_z + J_{xz}\dot{\omega}_x = \left(F_{yglf} + F_{ygrf}\right)a - \left(F_{yglr} + F_{ygrr}\right)b + \frac{\left(F_{xgrf} - F_{xglf}\right)c_f}{2} + \frac{\left(F_{xgrr} - F_{xglr}\right)c_r}{2} + \left(m_{ur}b - m_{uf}a\right)(\dot{v} + \omega_z u) \tag{3}$$

$$(J_x + mh_{rc}^2)\dot{\omega}_x + J_{xz}\dot{\omega}_z = mgh_{rc}\phi - \left(k_{\phi f} + k_{\phi r}\right)\phi - \left(b_{\phi f} + b_{\phi r}\right)\dot{\phi} + h_{rc}m(\dot{v} + \omega_z u) \tag{4}$$

where,

$$h_{rc} = \frac{h_{rcf}b + h_{rcr}a}{a+b}. \tag{5}$$

In these equations, the longitudinal force at the tire contact patch was denoted by F_{xgij}, the lateral force at the tire contact patch was denoted by F_{ygij}, and the subscript 'ij' denotes left front (*lf*), right front (*rf*), left rear (*lr*), and right rear (*rr*), respectively. The total mass of the vehicle is denoted by m_t, the distance of vehicle center of mass (C.M.) from front axle by a, the distance of the vehicle C.M. from rear axle by b, the forward velocity, lateral velocity, and the vertical velocity of the vehicle C.M. by u, v and w, the roll angle by ϕ, the roll inertial by J_x, the yaw inertial by J_z, the product of roll and yaw inertial by J_{xz}, the front and rear roll center distance below sprung mass C.M. by h_{rcf} and h_{rcr}, the front/rear unsprung mass by m_{uf} and m_{ur}, the front/rear track width by c_f and c_r. The front and rear suspensions are represented simply by their respective equivalent roll stiffness ($k_{\psi f}/k_{\psi r}$) and roll damping coefficients ($b_{\psi f}/b_{\psi r}$). We should notice that the roll DOF equation, i.e., Eq.(4), is given by considering moments about the vehicle roll center h_{rc}, rather than the sprung mass C.M.

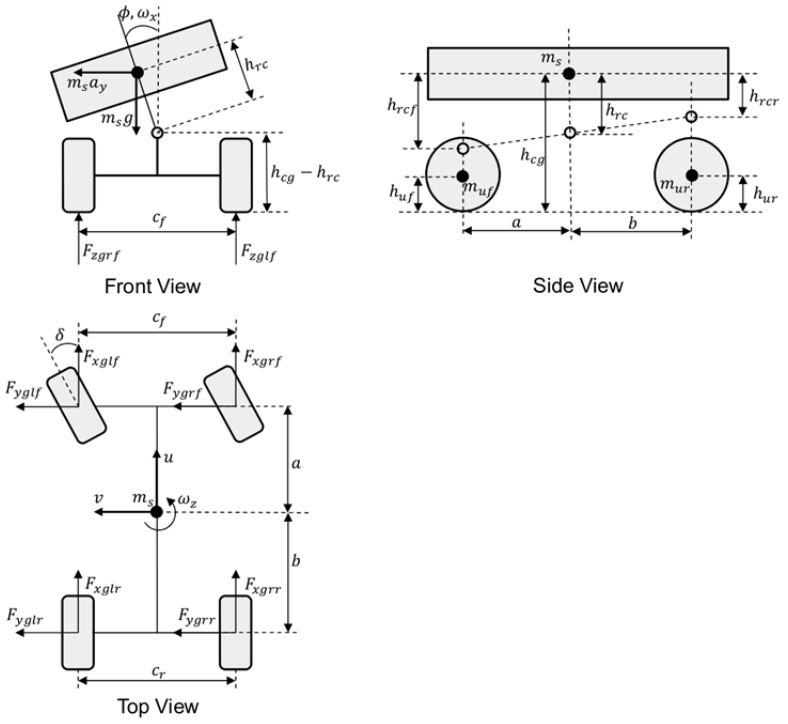

Figure 1. 8-DOF vehicle model [25].

2.3. 14-DOF vehicle model

Considering the suspension DOF at each corner, a 14-DOF vehicle model is capable of modeling the vehicle pitch and heave motions, besides the same benefit of an 8-DOF vehicle model. A 14-DOF vehicle model is also suitable to consider nonlinear spring and damper and vehicle behavior response to normal tire forces. All these advantages make the 14-DOF model better represent the coupling effects of vehicle lateral, longitudinal, roll and yaw motion, particularly during extreme maneuvers. Furthermore, the 14-DOF model is capable of predicting vehicle response even after wheel lift-off and it is therefore suitable to be used in rollover prediction/prevention strategies [25].

The schematic of the 14-DOF model investigating the vehicle roll behavior is presented in Figure 2. The 14-DOF model includes 6 DOF at the vehicle C.M. and 2 DOF at each wheel. The body-fixed coordinates are attached at the vehicle C.M. and aligned in coordinate frame 1, i.e., the principal directions. The forward velocity, lateral velocity, and the vertical velocity of the sprung mass are indicated by u, v, w, respectively. The pitch angle, yaw angle and roll angle of the sprung mass are

denoted by θ, ψ, ϕ. The roll angular velocity, pitch angular velocity and yaw angular velocity are denoted by ω_x, ω_y and ω_z. The moments transmitted to the sprung mass along the ω_x, ω_y and ω_z directions are denoted by M_{xij}, M_{yij} and M_{zij} and the subscript 'ij' denotes left front (*lf*), right front (*rf*), left rear (*lr*), and right rear (*rr*), respectively [25].

According to Newton's laws, the equation of motion for the 6-DOF sprung mass of the 14-DOF model can now be written as [25],

$$m(\dot{u} + \omega_y w - \omega_z v) = \sum(F_{xsij}) + mgsin\theta \tag{6}$$

$$m(\dot{v} + \omega_z u - \omega_x w) = \sum(F_{ysij}) - mgsin\phi cos\theta \tag{7}$$

$$m(\dot{w} + \omega_x v - \omega_y u) = \sum(F_{zsij} + F_{dzij}) - mgcos\phi cos\theta \tag{8}$$

$$J_x\dot{\omega}_x = \sum(M_{xij}) + \frac{(F_{zslf} - F_{zsrf})c_f + (F_{zslr} - F_{zsrr})c_r}{2} \tag{9}$$

$$J_y\dot{\omega}_y = \sum(M_{yij}) + (F_{zslr} + F_{zsrr})b - (F_{zslf} + F_{zsrf})a \tag{10}$$

$$J_z\dot{\omega}_z = \sum(M_{zij}) + (F_{yslf} + F_{ysrf})a - (F_{yslr} + F_{ysrr})b + \frac{(-F_{xslf} + F_{xsrf})c_f + (-F_{xslr} + F_{xsrr})c_r}{2}, \tag{11}$$

where m is the sprung mass and the cardan angles θ, ψ, ϕ can be obtained by integrating the following equations [25],

$$\dot{\theta} = \omega_y cos\phi - \omega_z sin\phi \tag{12}$$

$$\dot{\psi} = \frac{\omega_y sin\phi}{cos\theta} + \frac{\omega_z cos\phi}{cos\theta} \tag{13}$$

$$\dot{\phi} = \omega_x + \omega_y sin\phi tan\theta + \omega_z cos\phi tan\theta. \tag{14}$$

More details about the development on 14-DOF vehicle model is specified in [25].

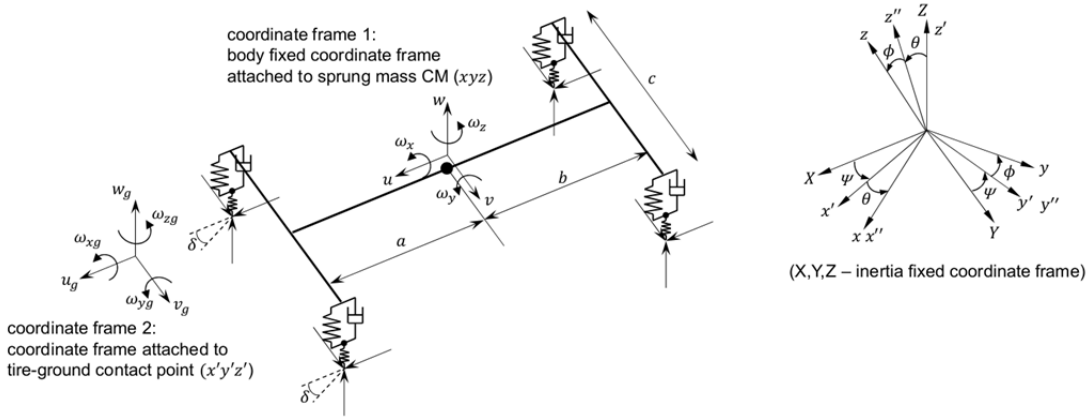

Figure 2. 14-DOF vehicle model with the coordinate frames [25].

2.4. Spatial-dependent vehicle model

In this study, in order to know the vehicle position explicitly at each sampling of the optimization routine and retain the capability of the solver to take into account the varied longitudinal velocity, we considered transforming a time-dependent model into a spatial-dependent model [26]. To this end, we introduce a spatial bicycle model to specify the transformation approach from time-dependent to spatial-dependent.

Figure 3 illustrates the curvilinear coordinate system used in the spatial bicycle model as well as the states of the vehicle model. The coordinate s defines the arc-length along the track. The states of

the spatial vehicle model are defined as $\xi^s = [\dot{y}, \dot{x}, \dot{\psi}, e_\psi, e_y]^T$, in which e_ψ and e_y are the errors of heading angle and lateral position respectively.

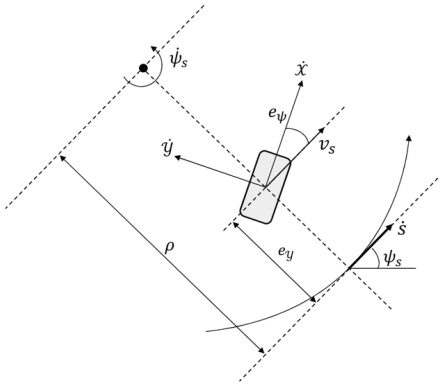

Figure 3. The curvilinear coordinate system [26].

The following kinematic equations can be derived from Figure 3 [26]

$$v_s = (\rho - e_y) \cdot \dot{\psi}_s \tag{15}$$

$$v_s = \dot{x} \cdot cos(e_\psi) - \dot{y} \cdot sin(e_\psi). \tag{16}$$

where v_s is the projected vehicle speed along direction of the path, ρ and ψ_s are the radius of curvature and the heading angle of the reference path. $\dot{\psi}_s$ is the time derivative of ψ_s.

Then the vehicle's velocity along the path $\dot{s} = \frac{ds}{dt}$ is written as [26]

$$\dot{s} = \rho \cdot \dot{\psi}_s = \frac{\rho}{\rho - e_y} \cdot \left(\dot{x}cos(e_\psi) - \dot{y} \cdot sin(e_\psi)\right). \tag{17}$$

where s is the projected vehicle position along the arc length of the path.

We obtain the derivative of ξ^s with respect to s using simple relationships in the new curvilinear coordinate system and the fact that $\frac{d\xi^s}{ds} = \frac{d\xi^s}{dt} \cdot \frac{dt}{ds}$. Then the spatial-dependent vehicle model is formulated as [26]:

$$\xi^{s\prime}(s) = f^s(\xi^s(s), u^s(s)). \tag{18}$$

In this paper, based on the above transformation, a spatial-dependent 8-DOF vehicle model will be employed as the prediction model in the formulation of MPC algorithm.

3. Coupled lateral and longitudinal controller design

Model predictive control aims to use a dynamic model to forecast system behavior, and optimize the control move at current time to bring the predicted output as close as possible to the given function. The computational burden will be increased with the increasement of system complexity. Compared with NMPC, we therefore utilize LMPC to design the coupled controller due to its advantages of simpler calculation and real-time performance.

In order to track the desired path and speed, we proposed an MPC-based path tracking with PID speed control to realize the coupled lateral and longitudinal control by a combined use of steering, accelerating and braking. In every simulation step, the longitudinal velocity in the prediction model is updated with measured value and the control input sequence is calculated by LMPC controller. Then, the driving or braking wheel torque is computed by PID controller using speed error between the plant and the reference. The optimal wheel steering angle and total wheel torque are passed to the plant simultaneously to track the desired path and speed. The schematic of the MPC-based path tracking with PID speed control is illustrated in Figure 4.

3.1. Lateral dynamics control

We use LMPC approach to implement the vehicle lateral control and a linearized 8-DOF vehicle model as the prediction model in the formulation of model predictive control algorithm.

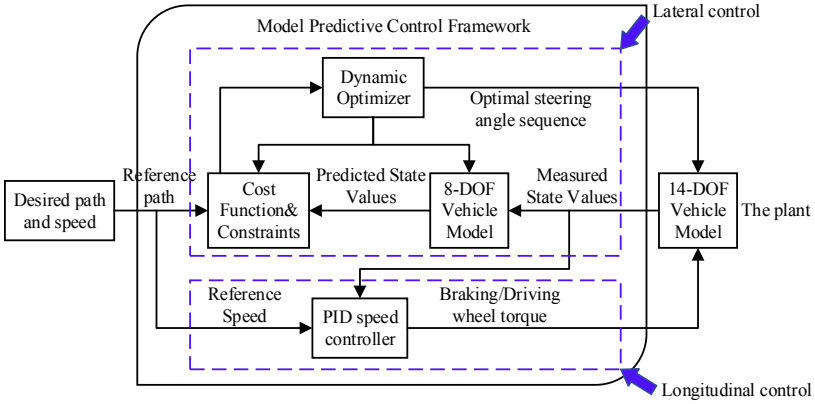

Figure 4. Schematic of the MPC-based path tracking with PID speed control.

3.1.1. Linearization of the vehicle model. Given the control input $u = \delta$ and the state variable $\chi = [\dot{y}, \dot{x}, \psi, \dot{\psi}, Y, X]^T$, the general form of vehicle dynamics equations can be written as:

$$\dot{\chi} = f(\chi, u), \tag{19}$$

The equations around the operating point is given as:

$$\dot{\chi}_o = f(\chi_o, u_o). \tag{20}$$

Using the Taylor series expansion at the operating point and ignoring higher order terms, we can obtain [9]

$$\dot{\chi} = f(\chi_o, u_o) + \frac{\partial f(\chi, u)}{\partial \chi}\Big|_{\substack{\chi=\chi_o \\ u=u_o}} (\chi - \chi_o) + \frac{\partial f(\chi, u)}{\partial u}\Big|_{\substack{\chi=\chi_o \\ u=u_o}} (u - u_o) \tag{21}$$

Subtracting Eq.(20) from Eq.(21) results in

$$\dot{\tilde{\chi}} = A\tilde{\chi} + B\tilde{u}, \tag{22}$$

where $A = \frac{\partial f(\chi,u)}{\partial \chi}\Big|_{\substack{\chi=\chi_o \\ u=u_o}}$, $B = \frac{\partial f(\chi,u)}{\partial u}\Big|_{\substack{\chi=\chi_o \\ u=u_o}}$, $\dot{\tilde{\chi}} = \dot{\chi} - \dot{\chi}_o$, $\tilde{\chi} = \chi - \chi_o$, $\tilde{u} = u - u_o$.

In order to apply this model to the MPC controller, we describe the equation in the form of discretized state-space representation [9]:

$$\chi(k+1) = A_d\chi(k) + B_d u(k) + d_k(k), \tag{23}$$

where $A_d = I + TA$, $B_d = TB$, $d_k(k) = f(\chi_o(k), u_o(k)) - (A_d\chi_o(k) + B_d u_o(k))$ and T is the sampling time.

3.1.2. State prediction. Defining new state variable $\xi(k) = \begin{bmatrix} \chi(k) \\ u(k-1) \end{bmatrix}$, the output state variable $\eta(k)$ and the control input increment $\Delta u(k) = u(k) - u(k-1)$, we can obtain a new form of the discrete state-space controller model [9]

$$\begin{aligned} \xi(k+1) &= \tilde{A}_d\xi(k) + \tilde{B}_d\Delta u(k) + \tilde{d}_k(k) \\ \eta(k) &= \tilde{C}_d\xi(k), \end{aligned} \tag{24}$$

where $\tilde{A}_d = \begin{bmatrix} A_d & B_d \\ 0_{m\times n} & I_m \end{bmatrix}$, $\tilde{B}_d = \begin{bmatrix} B_d \\ I_m \end{bmatrix}$, $\tilde{d}_k(k) = \begin{bmatrix} d_k(k) \\ 0_m \end{bmatrix}$, $\tilde{C}_d = [C_d \quad 0_{p\times m}]$ (m is the dimension of control input, n is the dimension of state variable, and p is the dimension of output).

The predicted state output over the prediction horizon N_p in a compact matrix form is given as

$$\eta_m(k) = \Theta_m\xi(k) + \Gamma_m\Delta U_m + \Psi_m D_k, \tag{25}$$

where

$$
\begin{aligned}
\Theta_m &= \begin{bmatrix} \tilde{C}_d\tilde{A}_d & \tilde{C}_d\tilde{A}_d^2 & \dots & \tilde{C}_d\tilde{A}_d^{N_c} & \dots & \tilde{C}_d\tilde{A}_d^{N_p} \end{bmatrix}^T \\
\eta_m(k) &= [\eta(k+1) \quad \dots \quad \eta(k+N_p)]^T \\
\Delta U_m &= [\Delta u(k) \quad \dots \quad \Delta u(k+m) \quad \dots \quad \Delta u(k+N_c-1)]^T \\
D_k &= \begin{bmatrix} \tilde{d}_k(k) & \tilde{d}_k(k+1) & \dots & \tilde{d}_k(k+N_p-1) \end{bmatrix}^T \\
\Gamma_m &= \begin{bmatrix} \tilde{C}_d\tilde{B}_d & 0 & \cdots & 0 \\ \tilde{C}_d\tilde{A}_d\tilde{B}_d & \tilde{C}_d\tilde{B}_d & \cdots & 0 \\ \vdots & \vdots & \cdots & 0 \\ \tilde{C}_d\tilde{A}_d^{N_c-1}\tilde{B}_d & \tilde{C}_d\tilde{A}_d^{N_c-2}\tilde{B}_d & \cdots & \tilde{C}_d\tilde{B}_d \\ \vdots & \vdots & \cdots & \vdots \\ \tilde{C}_d\tilde{A}_d^{N_p-1}\tilde{B}_d & \tilde{C}_d\tilde{A}_d^{N_p-2}\tilde{B}_d & \cdots & \tilde{C}_d\tilde{A}_d^{N_p-N_c}\tilde{B}_d \end{bmatrix} \\
\Psi_m &= \begin{bmatrix} \tilde{C}_d & 0 & 0 & \cdots & 0 \\ \tilde{C}_d\tilde{A}_d & \tilde{C}_d & 0 & \cdots & 0 \\ \tilde{C}_d\tilde{A}_d^2 & \tilde{C}_d\tilde{A}_d & \tilde{C}_d & \cdots & 0 \\ \vdots & \vdots & \vdots & \cdots & \vdots \\ \tilde{C}_d\tilde{A}_d^{N_p-1} & \tilde{C}_d\tilde{A}_d^{N_p-2} & \tilde{C}_d\tilde{A}_d^{N_p-3} & \cdots & \tilde{C}_d \end{bmatrix}.
\end{aligned}
$$

3.1.3. Cost function definition. The ability of the cost function is to make the autonomous vehicle track the desired path rapidly and smoothly. Therefore, the system status deviation and the optimization of the control output should be combined into the controller.

Considering the soft constraints concept [27], the objective function of the path tracking controller can be given as [9]:

$$J(k) = \sum_{i=1}^{N_p} \| \eta(k+i|t) - \eta_{ref}(k+i|t) \|_Q^2 + \sum_{i=1}^{N_c} \| \Delta U(k+i|t) \|_R^2 + \rho\varepsilon^2. \tag{26}$$

Considering Eq.(25), the objective function can be given as [9]

$$
\begin{aligned}
J(k) = \quad & \left(\Theta_m\xi(k) + \Gamma_m\Delta U_m + \Psi_m\tilde{d}_k - \eta_{ref}\right)^T Q\left(\Theta_m\xi(k) + \Gamma_m\Delta U_m + \Psi_m\tilde{d}_k - \eta_{ref}\right) \\
& + {\Delta U_m}^T R\Delta U_m + \rho\varepsilon^2.
\end{aligned} \tag{27}
$$

To solve the following optimization problem, the objective function is converted into a standard quadratic form [9].

$$J(\xi(t), u(t-1), \Delta U(t)) = [\Delta U(t)^T, \varepsilon]^T H_t [\Delta U(t)^T, \varepsilon] + G_t [\Delta U(t)^T, \varepsilon], \tag{28}$$

where $H_t = \begin{bmatrix} \Gamma_m^T Q \Gamma_m + R & 0 \\ 0 & \rho \end{bmatrix}$, $G_t = [2e_t^T Q\Gamma_m \quad 0]$, $e_t = (\Theta_m\xi(k) + \Psi_m\tilde{d}_k - \eta_{ref})$ and e_t is the tracking error in the predictive horizon .

3.1.4. Constraint analysis. In a real physical system, the control input and state output are bounded with actuator saturation and physical limitations. The constrains imposed on the control sequence and the state outputs can be described as follows [9]:

1. The constraints imposed on control input u are given as
$$u_{min}(t+k) \le u(t+k) \le u_{max}(t+k), \quad k = 0,1,\cdots,N_c-1 \tag{29}$$
2. The constraints imposed on control increments Δu are given as
$$\Delta u_{min}(t+k) \le \Delta u(t+k) \le \Delta u_{max}(t+k), \quad k = 0,1,\cdots,N_c-1 \tag{30}$$
3. The constraints imposed on the output y are given as
$$y_{min}(t+k) \le y(t+k) \le y_{max}(t+k), \quad k = 0,1,\cdots,N_c-1 \tag{31}$$

Since the variables to be solved are control increments in the control horizon, the constraints should be written in the form of control increment or the form of control increment multiplied by the transformation matrix. Thus, the constraints listed above should be converted to obtain the transformation matrix, which is described as [9]:

$$u(t+k) = u(t+k-1) + \Delta u(t+k), \tag{32}$$

assuming that

$$U_t = 1_{Nc} \otimes u(k-1) \tag{33}$$

$$A = \underbrace{\begin{bmatrix} 1 & 0 & \cdots & \cdots & 0 \\ 1 & 1 & 0 & \cdots & 0 \\ 1 & 1 & 1 & \ddots & 0 \\ \vdots & \vdots & \ddots & \ddots & 0 \\ 1 & 1 & \cdots & 1 & 1 \end{bmatrix}}_{N_c \times N_c} \otimes I_m \tag{34}$$

where 1_{N_c} is the column vector of N_c ones, I_m is the identity matrix with a dimension of m, $\otimes$ is Kronecker product, and $u(k-1)$ is the previous control input [9].

Combining Eq.(32) through (34) can be converted into [9]

$$U_{min} \leq \quad A\Delta U_t + U_t \leq U_{max}, \tag{35}$$

where U_{min} and U_{max} are the lower and upper bound of the control input, respectively.

Combining Eq.(25) and Eq.(31), the output constraints can be given as:

$$Y_{min} \leq \Theta_m \xi(k) + \Gamma_m \Delta U_m + \Psi_m D_k \leq Y_{max}, \tag{36}$$

After obtaining the solution of optimization for cost function, the control increments sequence in the control horizon can be given as [9]

$$\Delta U_t^* = [\Delta u_t^*, \Delta u_{t+1}^*, \dots, \Delta u_{k+N_c-1}^*]^T. \tag{37}$$

The first element of the sequences is taken as the actual control input increment, thus the control input signal is given as:

$$u(t) = u(t-1) + \Delta u_t^*. \tag{38}$$

3.2. Longitudinal dynamics control.

The wheel rotational dynamics of front right and rear right wheel in the plant are given as [28],

$$J_w \dot{\omega}_{rf} \quad = T_{arf} - T_{brf} - r_{rf} F_{xtrf} \tag{39}$$

$$J_w \dot{\omega}_{rr} \quad = -T_{brr} - r_{rr} F_{xtrr}, \tag{40}$$

where the T_{arf} and T_{brf} is driving torque and braking torque applied to the front right wheel. T_{brf} is braking torque applied to the rear right wheel. For simplicity, we assume the driving torque is divided equally to front two wheels and the braking torque is divided equally to the front and rear four wheels.

The longitudinal velocity and acceleration of the plant model can be obtained by considering a simplified one-wheel vehicle model and the longitudinal motion equation for the chassis of 14-DOF vehicle model.

As it is known to us, most industrial controllers in use today are PID controllers or modified PID controllers. The usefulness of PID controls lies in their general applicability to most control systems. Herein, we implement the longitudinal controller using the PID controller.

The speed tracking error is defined as

$$e_u \quad = u_d - u \tag{41}$$

$$e_{\dot{u}} \quad = \dot{u}_d - \dot{u} \tag{42}$$

$$e_{s_x} \quad = \int_{t_1}^{t_2} e_u \, dt = e_u T_s, \tag{43}$$

where u_d refers to the desired speed, u refers to the speed of the plant; $\dot{u}_d$ refers to the desired longitudinal acceleration, $\dot{u}$ refers to the longitudinal acceleration of the plant. T_s is the sample time and when using the arc length dependent model, $T_s = \Delta s / \dot{s}$.

In the PID controller, when the speed of the plant vehicle is smaller than the desired speed, then $T_a = K_P e_u + K_I e_{s_x} + K_D e_{\dot{u}}$, $T_b = 0$; when the speed of the plant is greater than the desired speed,

then $T_b = K_P e_u + K_I e_{s_x} + K_D e_{\dot{u}}$, $T_a = 0$; when the speed of the plant equals to the desired speed, then $T_a = 0, T_b = 0$.

4. Simulation results

In this part, we firstly validated the developed vehicle models by comparing the output responses with CarSim vehicle model using step steering input. Then, we implement the proposed controller for combined lateral and longitudinal control considering the references path to be an 8-shaped curve trajectory.

4.1. Vehicle model validation

It is important to use a precise and accurate model for the development of a control system. Thus, the developed vehicle models should be validated before implementing the path tracking control and speed tracking control. CarSim is a software with plenty of high-fidelity vehicle models that has been validated with experimental results on an actual vehicle. Herein, we compare the simulation result of steering response with that of CarSim vehicle model to investigate the validation.

Assuming the longitudinal velocity is constant in the simulation, we apply the same road-wheel steering angle as input signal to the 8-DOF model, the 14-DOF model and the CarSim model to implement the step steering simulation.

Step steering simulation: the amplitude of step steering angle is 0.0087(rad), i.e., 0.5(deg) and the vehicle longitudinal velocity is constant at 33.73(m/s). The output responses of the vehicle models including roll angle, yaw rate, lateral velocity and lateral acceleration are presented in Figure 5 and Figure 6 as follows:

(1) Comparison of step steer simulation between 8-DOF vehicle model and CarSim model

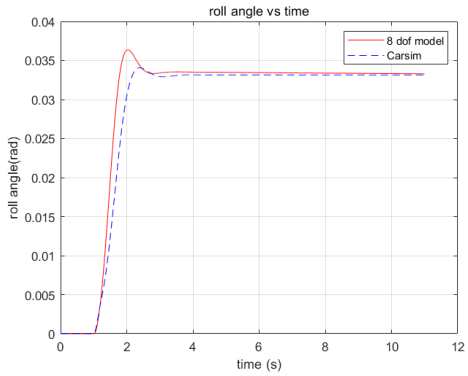

(a). Comparison of vehicle roll angle

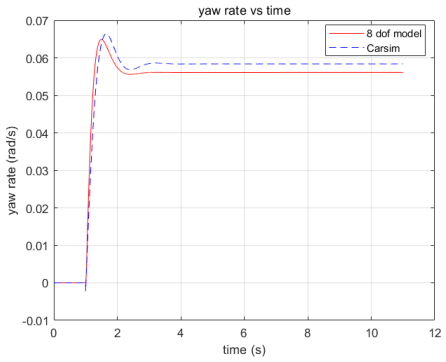

(b). Comparison of vehicle yaw rate.

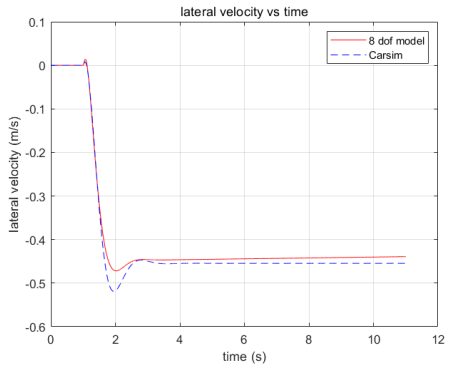

(c). Comparison of lateral velocity.

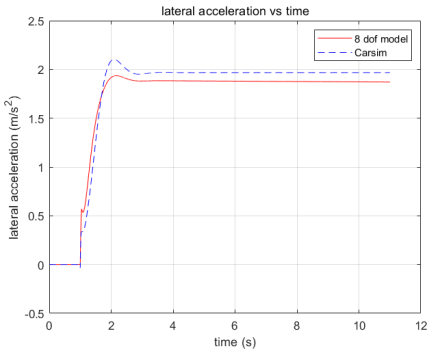

(d). Comparison of lateral acceleration

Figure 5. Comparison between 8-DOF model and CarSim during step steering at a speed of 33.73m/s.

(2) Comparison of step steer simulation between 14-DOF vehicle model and CarSim model

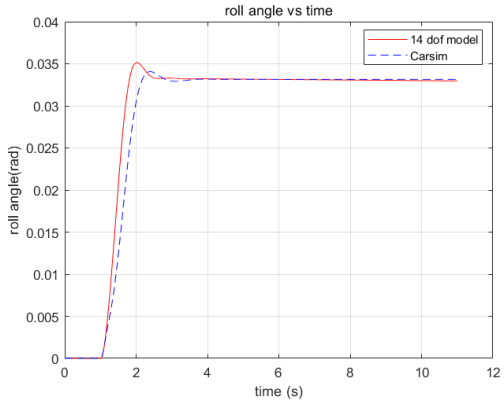

(a). Comparison of vehicle roll angle

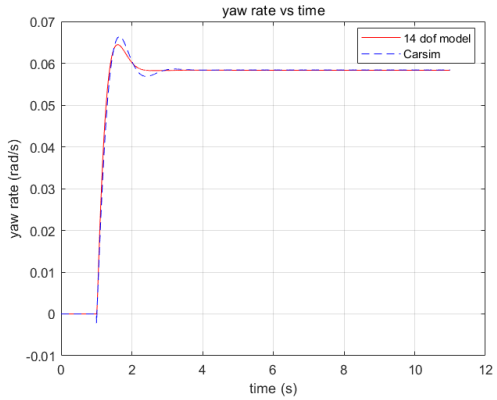

(b). Comparison of vehicle yaw rate.

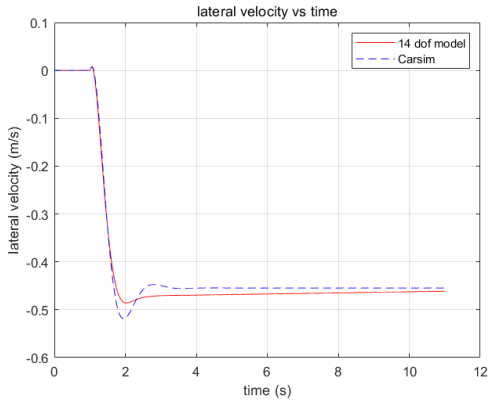

(c). Comparison of lateral velocity.

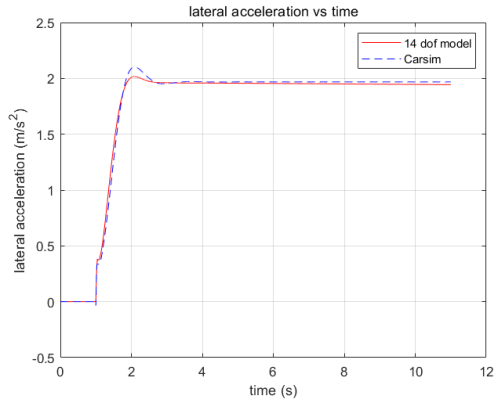

(d). Comparison of lateral acceleration

Figure 6. Comparison between 14-DOF model and CarSim during step steering at a speed of 33.73m/s.

Based on the simulation results, the output responses of the 8-DOF vehicle model and the 14-DOF vehicle model are reasonable and approximate to the simulation results of CarSim vehicle model. It is also shown that the 14-DOF vehicle model correlates better with CarSim model than the 8-DOF vehicle model during steady state in terms of vehicle roll angel, yaw rate, lateral velocity and lateral acceleration. Thus, the developed vehicle models can be used in the formulation of model predictive control algorithm.

4.2. Tracking reference definition

We employ an 8-shaped curved reference trajectory with time-varied speed to investigate the path tracking and speed tracking performance in the situation of curved road. The reference path is an 8-shaped curved path with a straight line. The vehicle first drives on a straight line with the speed increased from $0.5m/s$ to $10m/s$, and then drives along the 8-shaped curved path with a radius of $30m$ and a constant speed. The reference trajectory and the reference speed profile with respect to the arc length are defined in Figure 7:

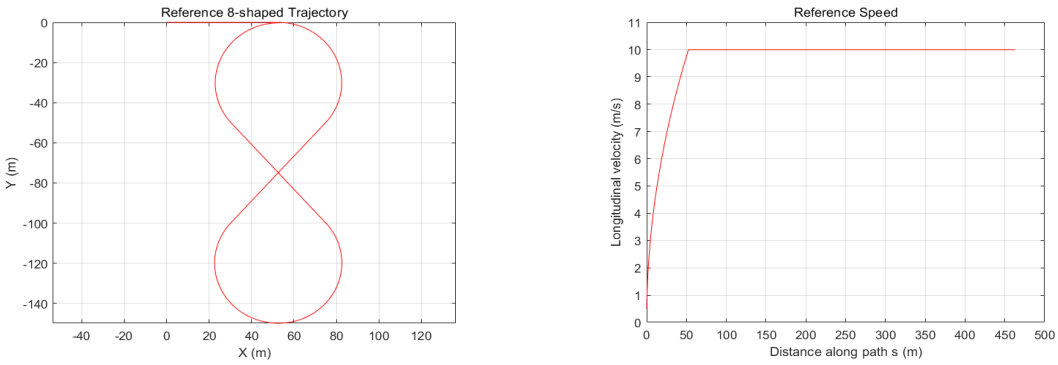

(a). Reference trajectory **(b).** Reference speed

Figure 7. Definition of reference trajectory and vehicle speed.

4.3. Tracking performance simulation

In the formulation of model predictive path tracking controller, the 8-DOF vehicle model is used as the prediction model and the 14-DOF vehicle model is used as the plant model. In the cost function, we choose the heading angle 'ψ', the lateral position 'Y' and the longitudinal position 'X' of vehicle C.M. in global coordinates as the tracking objectives. Based on the proposed coupled control scheme, we implement the path tracking and speed control by the use of combined lateral and longitudinal control. The tracking performance of our proposed controller are illustrated as follows:

(1) Compared with the reference values, the tracking performances of vehicle state variables including the lateral position 'Y', the longitudinal position 'X', the heading angle 'ψ' and the yaw rate '$\dot{\psi}$' are presented in Figure 8:

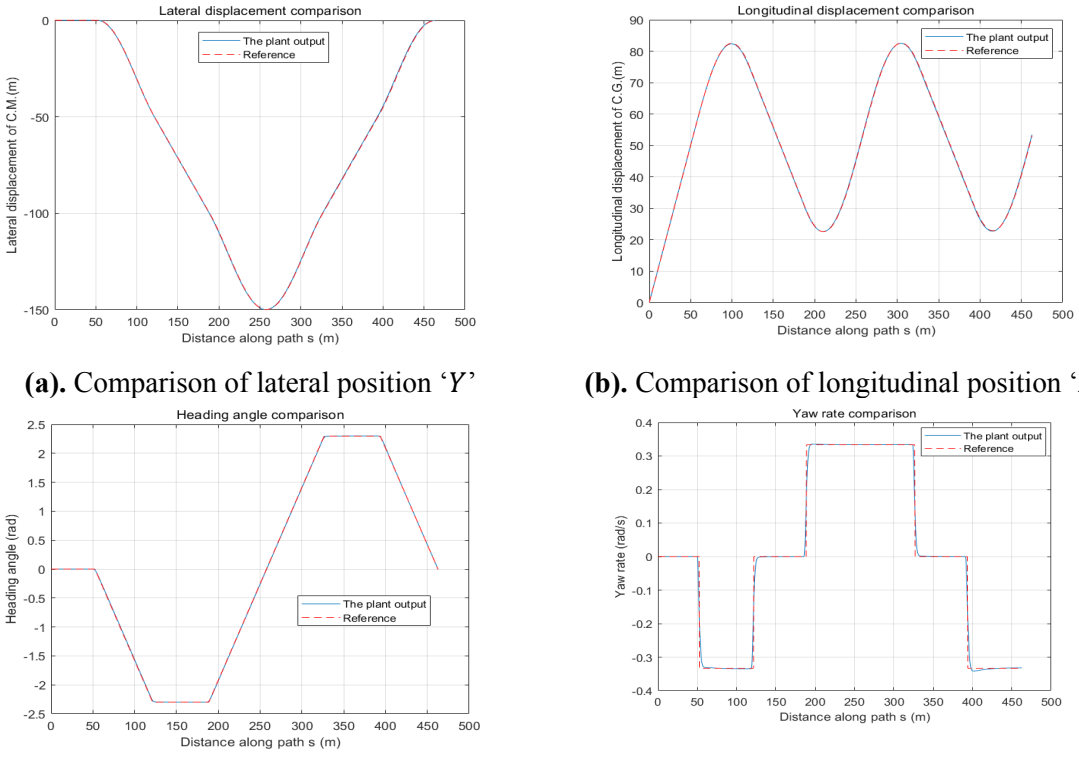

(a). Comparison of lateral position 'Y' **(b).** Comparison of longitudinal position 'X'

(c). Comparison of heading angle 'ψ' **(d).** Comparison of vehicle yaw rate '$\dot{\psi}$'

Figure 8. Tracking performance of vehicle state variables.

(2) Compared with the reference trajectory and speed profile, the path tracking performance and the speed tracking performance of the proposed coupled controller for lateral and longitudinal control are illustrated in Figure 9:

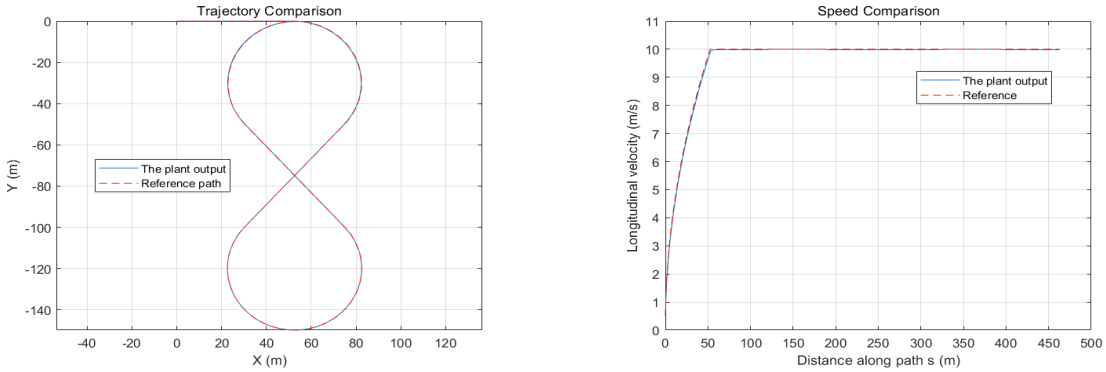

(a). Comparison of tracking trajectory **(b).** Comparison of tracking speed

Figure 9. Tracking performance of 8-shaped trajectory and vehicle speed.

(3) The control input of front wheel steering angle and total driving/braking wheel torque are illustrated in Figure 10:

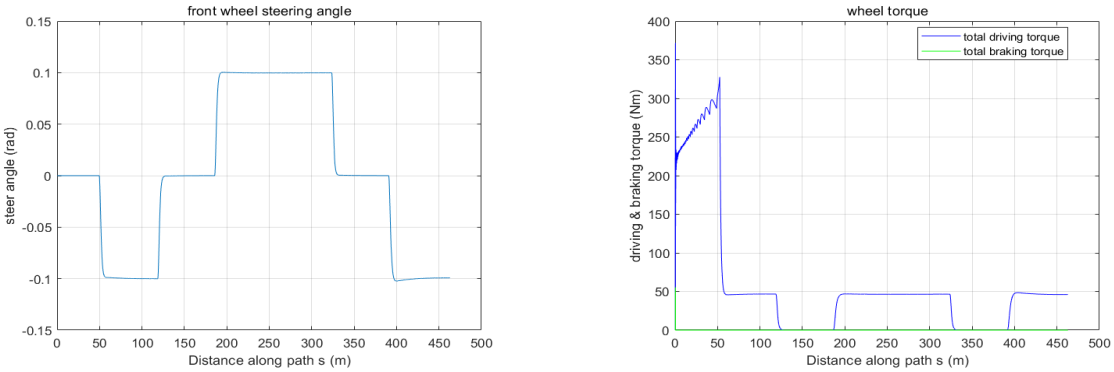

(a). Front wheel steering angle input **(b).** Driving/braking wheel torque input

Figure 10. Control input signals for the path tracking and speed control.

Table 1. Path tracking and speed tracking errors with 8-shaped curved trajectory.

Vehicle state	Lateral position	Longitudinal position	Heading angle	Yaw rate	Longitudinal velocity
	$Y(m)$	$X(m)$	$\psi(rad)$	$\dot{\psi}(rad/s)$	$\dot{x}\ (m/s)$
Tracking error*	0.6497	0.3932	0.0280	0.1695	0.1319

* The maximum absolute tracking error along the path.

(4) Numeral tracking errors of the vehicle state variables are summarized and given in Table 1:

In this section, we implement the proposed MPC-based path tracking with PID speed control to address the coupled lateral and longitudinal control problem, in which the 8-DOF vehicle model is used as the prediction model, and the high-fidelity model, i.e., the 14-DOF vehicle model is used as the plant model. In order to consider the time-varied speed in the path tracking, a PID speed controller is embedded in the model predictive control framework. Based on the simulation results, the proposed

controller shows good tracking performance of following the desired path and the desired speed by the use of combined lateral and longitudinal control. Considering the 8-shaped trajectory with a radius of $30m$, the tracking errors between the plant and the objectives for the heading angle 'ψ', yaw rate '$\dot{\psi}$', lateral position 'Y', longitudinal position 'X' and the vehicle speed '$\dot{x}$' are relatively small, which are shown in Figure 8, Figure 9 and Table 1.

5. Conclusions and future work

In the literature of path tracking, numerous researches implemented the lateral guidance of autonomous vehicles with the assumption of constant speed, so that the lateral and longitudinal control problem can be investigated in a decoupled way. However, the automotive vehicle is nonlinear system with strong couplings between the longitudinal and lateral motion, moreover, the speed is usually varied along the trajectory. Thus, in this paper, we proposed a novel MPC-based path tracking with PID speed control to deal with the coupled lateral and longitudinal vehicle dynamics. We used an 8-DOF vehicle model as the prediction model and used a high-fidelity model, i.e., a 14-DOF vehicle model to approximate the plant. In order to know explicitly the vehicle position at each sampling instant of an optimization and maintain the freedom of the solver to time-varied speed, we transformed the time-dependent model to spatial-dependent model to formulate the LMPC algorithm. The path tracking controller generated the optimal road-wheel steering angle and the PID speed controller embedded in the solution generated the total accelerating or braking wheel torque. All these control input signals were passed to the plant model simultaneously to realize the coupled control of path tracking and speed tracking. Furthermore, we considered an 8-shaped curved path as the reference path to investigate the tracking performance of the proposed controller in curved road situation. Based on the simulation results, we report relatively small tracking errors between the plant and the reference objectives for the heading angle 'ψ', yaw rate '$\dot{\psi}$', lateral position 'Y' and longitudinal position 'X' of vehicle C.M. The proposed coupled controller presents good tracking performance of following the reference path and speed.

In the future work, we will consider the reference path to be an arbitrary curve of continuously varying curvature and implement the combined lateral and longitudinal control using the coupled controller. Furthermore, we will consider generating a reference speed profile for optimal time travel along the predefined trajectory.

References

[1] G. Tagne, R. Talj, A. Charara 2016 Design and Comparison of Robust Nonlinear Controllers for the Lateral Dynamics of Intelligent Vehicles *IEEE Transactions on Intelligent Transportation Systems* **17(3)** 796-809

[2] K. Liu, J. Gong, S. Chen, et al. 2018 Dynamic Modeling Analysis of Optimal Motion Planning and Control for High-speed Self-driving Vehicles *Journal of Mechanical Engineering* **54(14)** 141-151

[3] X. Zhao, H. Chen 2011 A study on lateral control method for the path tracking of intelligent vehicles *Automotive Engineering* **33(5)** 382-387

[4] R. Marino, S. Scalzi, M. Netto 2011 Nested PID steering control for lane keeping in autonomous vehicles *Control Engineering Practice* **19(12)** 1459 -1467

[5] Y. Ma, K. Li, F. Gao, et al. 2006 Design of an improved optimal preview lateral controller *Automotive Engineering* **28(5)** 433-438

[6] C. Hu, R. Wang, F. Yan, et al. 2016 Output Constraint Control on Path Following of Four-Wheel Independently Actuated Autonomous Ground Vehicles *IEEE Transactions on Vehicular Technology* **65(6)** 4033-4043

[7] A. Norouzi, M. Masoumi, A. Barari, et al. 2019 Lateral control of an autonomous vehicle using integrated backstepping and sliding mode controller *Proceedings of the Institution of Mechanical Engineers, Part K: Journal of Multi-body Dynamics* **233(1)** 141-151

[8] J. Wang, W. Chen, T. Wang, et al. 2012 Vision guided intelligent vehicle lateral control based

on desired yaw rate *Journal of Mechanical Engineering* **48(4)** 108-115
[9] J. Gong, Y. Jiang, W. Xu, K. Liu, H. Guo, and Y. Sun. 2015 Multi-constrained model predictive control for autonomous ground vehicle trajectory tracking *Journal of Beijing Institute of Technology* **24(4)** 441-448
[10] K. Liu, J. Gong, A. Kurt, et al. 2018 Dynamic modeling and control of high-speed automated vehicle for lane change maneuver *IEEE Transactions on Intelligent Vehicles* **3(3)** 329-339
[11] P. Falcone, H. Tseng, F. Borrelli, J. Asgari, and D. Hrovat. 2008 MPC-based yaw and lateral stabilisation via active front steering and braking *Vehicle System Dynamics* **46(S1)** 611-628
[12] T. Ming, W. Deng, S. Zhang, and B. Zhu. 2016 MPC-based trajectory tracking control for intelligent vehicles *SAE Technical Paper* **2016-01-0452**
[13] R. Attia, R. Orjuela, and M. Basset. 2014 Combined longitudinal and lateral control for automated vehicle guidance *Vehicle System Dynamics* **52(2)** 261-279
[14] F. Lin, Y. Zhang, Y. Zhao, et al. 2019 Trajectory tracking of autonomous vehicle with the fusion of DYC and longitudinal lateral control *Chinese Journal of Mechanical Engineering* **32** 16
[15] D.R. Mikesell 2008 Portable automated driver for universal road vehicle dynamics testing The Ohio State University, US
[16] E.M. Lim, J.K. Hedrick 1999 Lateral and longitudinal vehicle control coupling for automated vehicle operation *Proceedings of the American Control Conference* San Diego, CA, US: 3676 -3680
[17] E.M. Lim 1998 Lateral and longitudinal vehicle control coupling in the automated highway system University of California at Berkeley, US
[18] L. Menhour, B. d'Andréa-Novel, C. Boussard, et al. 2011 Algebraic nonlinear estimation and flatness-based lateral/longitudinal control for automotive vehicles *14th International IEEE Conference on Intelligent Transportation Systems (ITSC).* Washington, DC, US: 463-468
[19] L. Nehaoua, L. Nouvelière 2012 Backstepping based approach for the combined longitudinal-lateral vehicle control *IEEE Intelligent Vehicles Symposium* (*IV'12*). Spain: Alcalá de Henares: 395-400
[20] J. Guo, P. Hu, R. Wang. 2016 Nonlinear coordinated steering and braking control of vision-based autonomous vehicles in emergency obstacle avoidance *IEEE Transactions on Intelligent Transportation Systems* **17(11)** 3230–3240
[21] M.G. Plessen, D. Bernardini, H. Esen, et al. 2018 Spatial-Based Predictive Control and Geometric Corridor Planning for Adaptive Cruise Control Coupled With Obstacle Avoidance *IEEE Transactions on Control System Technology* **26(1)** 38-50
[22] A.F. Idriz, A.S. Rachman, S. Baldi 2017 Integration of auto-steering with adaptive cruise control for improved cornering behavior *IET Intelligent Transport Systems* **11(10)** 667-675
[23] A. Chebly, R. Talj, A. Charara 2019 Coupled longitudinal/lateral controllers for autonomous vehicles navigation, with experimental validation *Control Engineering Practice* **88** 79-96
[24] F. Borrelli, P. Falcone, T. Keviczky, et al. 2005 MPC-based approach to active steering for autonomous vehicle systems *International Journal of Vehicle Autonomous Systems* **3(2)** 265-291
[25] T. Shim, C. Ghike 2007 Understanding the limitations of different vehicle models for roll dynamics studies *Vehicle System Dynamics* **45(3)** 191-216
[26] Y. Gao, A. Gray, J. V. Frasch, et al. 2012 Spatial predictive control for agile semi-autonomous ground vehicles *Proceedings of the 11th International Symposium on Advanced Vehicle Control*
[27] S. Li, J. Wang, K. Li 2010 Stabilization of linear predictive control systems with softening constraints *Journal of Tsinghua University* (*Science and Technology*) **50 (11)** 1848-1852
[28] J. He, D.A. Crolla, M.C. Levesley, et al. 2004 Integrated active steering and variable torque distribution control for improving vehicle handling and stability *SAE Technical Paper* **2004-01-1071**